ELSEVIER

Journal of Atmospheric and Solar-Terrestrial Physics 69 (2007) 1233–1240

Journal of ATMOSPHERIC AND SOLAR-TERRESTRIAL PHYSICS

www.elsevier.com/locate/jastp

Prompt response of SAPS to stormtime substorms

E.V. Mishin[a,*], V.M. Mishin[b]

[a]*Boston College Institute for Scientific Research, 402 St Clements Hall, 140 Commonwealth Avenue, Chestnut Hill, MA 02467, USA*
[b]*Institute of Solar-Terrestrial Physics, SB RAS, P.O. Box 4026, Irkutsk 664033, Russia*

Received 13 April 2006; received in revised form 24 July 2006; accepted 18 September 2006
Available online 27 March 2007

Abstract

We report on satellite, incoherent scatter radar, and ground magnetometer observations of the development of SAPS during a stormtime substorm event on 25 September 1998. The substorm onset was determined from the data of the ground magnetometer array and LANL satellites. The radar and Defense Meteorological Satellite Program (DMSP) satellites identified the SAPS region. The pre-existing SAPS in the afternoon sector moved equatorward and intensified within ~10 min after the substorm onset. It is shown that this transition began when the westward traveling surge (WTS) arrived at the adjacent auroral region. The observations indicate that the stormtime ring current responds to the substorm expansion on a rapid timescale, characteristic for the dipolarization pulse and WTS development. A scenario for the generation of the post-onset SAPS-wave structures is proposed.

Keywords: SAPS; Prompt response; Stormtime substorm

1. Introduction

Latitudinally narrow streams of enhanced sunward convection ($V_W > 0.5$ km/s), dubbed polarization jets (Galperin et al., 1974) or subauroral ion drifts (SAID) (Spiro et al., 1979; Anderson et al., 1993), are well-known subauroral signatures of magnetic activity. They are driven by poleward electric fields intensified in a low-conductance ionosphere conjugate to the ring current-plasmasphere overlap. SAID are considered as a subset of the subauroral polarization streams (SAPS) that include plasma flow events both broad and narrow extents in latitude (Foster and Burke, 2002). Sometimes, SAPS are highly variable and structured (Maynard et al., 1980; Erickson et al., 2002; Mishin et al., 2002, 2003a, 2004; Foster et al., 2004; Mishin and Burke, 2005). Especially strong SAPS-wave structures (SAPSWS), in which V_W-oscillations reach ±1–2 km/s and exceed the dc component, follow stormtime substorm onsets.

The features of SAPSWS depend on the timespan after substorm onsets. Fig. 1 shows the SAPSWS events along three successive orbits of the DMSP F8 satellite on 5 June 1991 beginning at ~16 : 35, 18 : 19, and 20 : 04 UT, respectively. The nearest in time substorm onsets occurred at ~15 : 15 and 16 : 54 UT. Note that the most equatorward boundary of the auroral zone was near −55° MLAT (Mishin and Burke, 2005). On average, the plasma density $\widehat{n}$ in the first $SAPSWS_1$ was not perturbed, however,

*Corresponding author. Tel.: +1 781 377 1309; fax: +1 781 37709950.
E-mail address: Evgenii.Mishin@hanscom.af.mil (E.V. Mishin).

1364-6826/$ - see front matter © 2007 Elsevier Ltd. All rights reserved.
doi:10.1016/j.jastp.2006.09.009

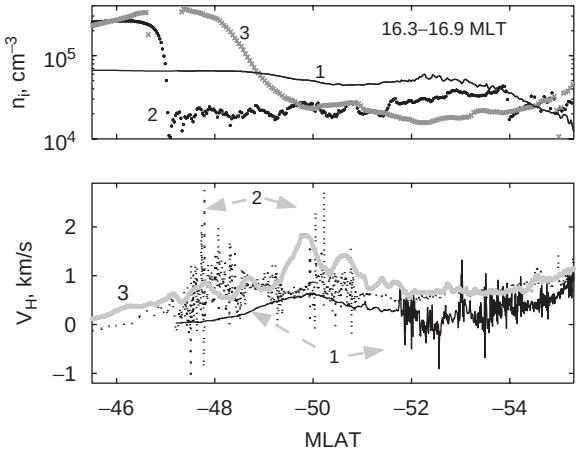

Fig. 1. Development of the SAPSWS over three successive orbits of the DMSP F8 satellite: 1-s averaged ion densities (top) and the horizontal component of convection velocities (bottom) versus the dipole MLat. 1, 2, and 3 indicate $SAPSWS_{1,2,3}$ near ~16 : 38, 18 : 20, and 20 : 05 UT, respectively.

there appeared distinct density irregularities $\delta n/\widehat{n} \leqslant 0.1$. The second $SAPSWS_2$, encountered after the subsequent onset, intensified and moved equatorward relative to the $SAPSWS_1$. A highly irregular, $\delta n/\widehat{n} \sim 0.3$, density trough was established. By the time of the third encounter, the SAPSWS transformed into a SAID-like structure remaining roughly at the same location. Strong oscillations in the convection velocity and density disappeared.

It is well known that enhanced ionospheric irregularities interfere communication and navigation. Irregularities intensify during magnetically perturbed periods, usually in the auroral ionosphere. During magnetic storms the auroral zone expands equatorward, and it is commonly believed that mid-latitude scintillation events occur inside the stormtime auroral zone. However, Basu et al. (2001) observed strong scintillations in 250-MHz signals well-equatorward of the expanded auroral oval. Similar mid-latitude scintillation events were also reported by Ledvina et al. (2002). Basu et al. (2001) noted that the DMSP F13 and F14 satellites had flown near the region of scintillations and observed highly structured convection flows at subauroral latitudes. Mishin et al. (2003b) analyzed the DMSP F13 and 14 overflights and found that the subauroral GPS scintillation events collocated with SAPSWS-related, highly-irregular troughs. Short-scale irregularities, the likely cause of the scintillations, seemed to develop and fade within about an hour after substorm onsets (cf. Fig. 1). Thus, specifying the post-onset dynamics of SAPS is important for predicting space weather effects at mid-latitudes (cf. Goldstein et al., 2005).

In this paper the SAPS's response to the substorm onset is determined from DMSP, LANL, incoherent scatter radar (ISR), and ground magnetometer observations during a stormtime substorm event on 25 September 1998. Mishin et al. (2002) (hereafter M2002) have already used some of these observations to study global ULF perturbations driven by variations in the solar wind dynamic pressure and IMF. Although M2002 noted that a pre-existing SAPS moved equatorward and intensified after the onset, consequences of that were not pursued. We show that this transition in the afternoon sector followed the arrival of the westward traveling surge at the adjacent auroral region and completed within ~10 min after the substorm onset.

2. Results

2.1. The substorm development

M2002 described the development of the storm initiated by an interplanetary shock at ~23 : 45 UT on 24 September 1998. Here we focus on a substorm at the beginning of the recovery phase when the ring current pressure was maximum near $L = 4$ (Liemohn et al., 2001). On average, the southward and azimuthal IMF components, solar wind velocity, AE and Dst indices were $\simeq 12$ and 13 nT, ~800 km/s, $\simeq 1500$ and −180 nT, respectively. The substorm onset near 08 : 18 UT was likely triggered by a brief northward turning of the southward IMF. Figs. 2 and 3 display the salient features of the substorm expansion phase.

Fig. 2 shows global-scale systems of equivalent currents in MLAT–MLT coordinates at 08 : 10 (top) and 08 : 30 UT. They are obtained from the data of globally distributed magnetometers by the magnetogram inversion technique MIT2 described in detail by Mishin (1991) and Mishin et al. (2000). Here heavy-reddish (thin-black) lines and the ± numbers inside vortices indicate clockwise (anticlockwise) rotation and current intensities in kA, respectively (the isolines are spaced by 80 kA). Stars and squares indicate the location of the LANL satellites and magnetic stations used in Fig. 3. The arrow and dashed line show the Irkutsk ISR backscatter region and the post-onset track of the DMSP F13 satellite, respectively. Apparently,

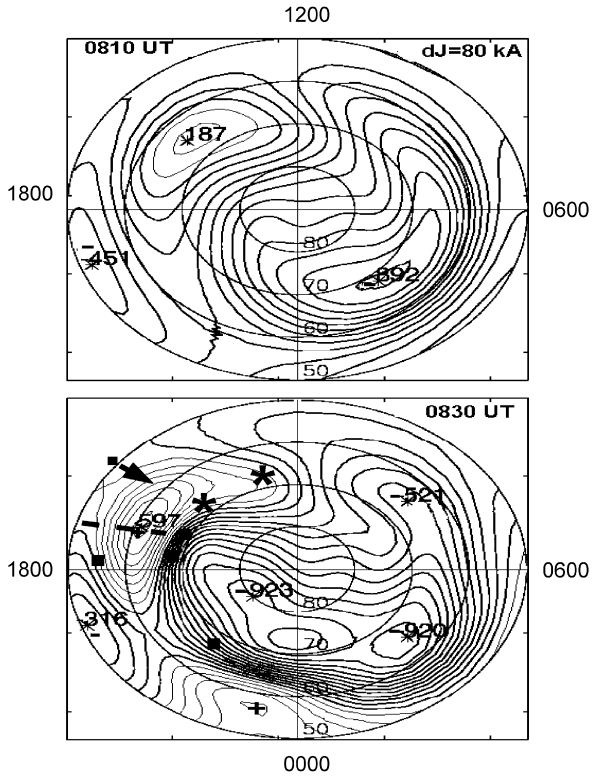

Fig. 2. The system of equivalent currents in MLAT–MLT coordinates at 08 : 10 (top) and 08 : 30 UT. Heavy (thin) lines indicate clockwise (anti-clockwise) direction. Shown in the center of vortices are total intensities in kA. The location of the LANL satellites (stars) and magnetic stations (squares) are indicated. The arrow and dashed line show the coherent backscatter region of the Irkutsk radar and the post-onset track of F13, respectively.

before the onset the current system is an example of a DP2 pattern, skewed because of the large azimuthal IMF. The post-onset currents are dominated by an enhanced westward electrojet in the evening/duskside auroral ($\Lambda > 63^\circ$) ionosphere, which is consistent with the substorm current wedge and westward traveling surge (WTS) concepts (e.g., Akasofu, 1977). In turn, eastward currents and thus poleward electric fields intensified in the adjacent ($\Lambda < 60^\circ$) subauroral ionosphere.

Top two panels in Fig. 3 show variations in energetic ion populations from the LANL-97A (~1300 MLT) and LANL 1994-084 (~1530 MLT) geostationary satellites, respectively. The vertical dashed line at ~08 : 19 : 30 UT in the second panel indicates dispersionless enhancements of the high-energy ($\varepsilon \geqslant 113$ keV) ion fluxes, the signature of a substorm injection at geosynchronous orbit (e.g., Thomsen et al., 2001). In turn, dispersive ion enhancements at 1300 MLT (top) are consistent with gradient-curvature drifting ions with the azimuthal speed $\sim 0.5\widetilde{L}^2\widetilde{\varepsilon}_\perp$(h − LT)/ min (the dipole approximation). Here $\widetilde{\varepsilon}_\perp = \varepsilon_\perp$[keV]/100, $\varepsilon_\perp$ is the perpendicular kinetic energy, and $\widetilde{L} = L/6.6$. However, note that at Dst~ − 200 nT the magnetic field in the dusk sector can substantially deviate from the dipole (e.g., Tsyganenko et al., 2003), thus hampering quantitative evaluations. At any rate, these features suggest (e.g., Birn et al., 1997; Liou et al., 2001) that the dipolarization pulse ceased soon after its arrival at 1530 MLT.

Pi2 (40–150 s) pulsations are one of the most popular indicators for substorm onsets, accurate to ~1 min (e.g., Liou et al., 2000). Furthermore, auroral Pi2 pulsations are closely associated with the initiation of the WTS (e.g., Pytte et al., 1976). Fig. 3 shows Pi2 waveforms obtained by applying 30–150-s bandpass filter to variations in the horizontal magnetic component H from Magadan (MGD, ~54 MLat), Chokurdakh (CHD, 65 MLat), Tixie Bay (TIK, 66 MLat) of the 210 MM network (Yumoto et al., 1996) and Dawson (DAW, 66 MLat) of the CANOPUS array. One can see that the magnitude of Pi2 pulsations at each site significantly increased after a local onset. Its MLT-time dependence resembles a westward traveling front, beginning near 21 MLT at ~08 : 19 UT and ending near 16 : 30 UT at ~08 : 23 : 30 UT. Overall, the magnetic observations suggest that at ≈ 08 : 24 UT the WTS reached its 'terminal' near 16 MLT and L~6.6. The lag ~5 min behind the Pi2 onset in the evening sector suggests the mean azimuthal speed in the magnetosphere ~1(h− LT)/ min, i.e. at the upper side of typical WTS velocities (cf. Rothwell et al., 1984).

Having identified the substorm onset and the WTS development, we turn to discuss the response of the SAPS.

2.2. The SAPS's response

Fig. 4 shows the SAPS pattern near 17 MLT along two successive orbits of the DMSP F13 satellite, beginning, respectively, at 07 : 44 (before the onset) and 09 : 26 UT (after). Here solid and dotted lines show the in-track (≃ poleward) electric component E_H and deviation from the IGRF model of the post-onset eastward magnetic component ΔB_Z (right axis), respectively. As anticipated, the SAPS was embedded within the region of the downward current ~0.5 μA/m^2. Likewise the SAPSWS$_2$ in Fig. 1, the SAPS region

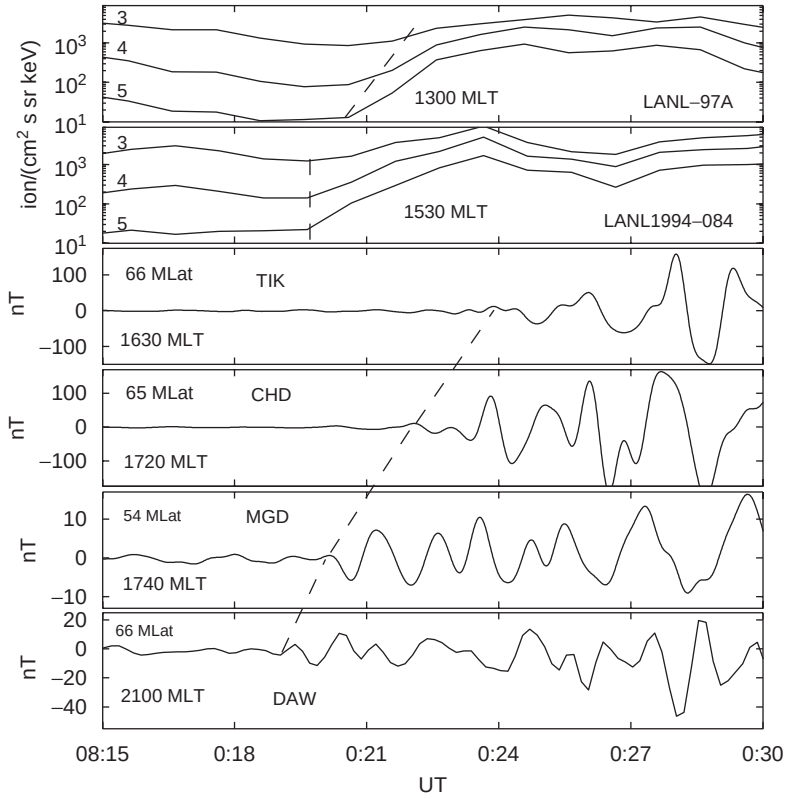

Fig. 3. (top and second) Differential ion fluxes in $1/(\mathrm{keV\,cm^2\,ster\,sec})$ from the LANL satellites. 3, 4, and 5 stand for energies $\varepsilon_\perp = 113-170$, 170–250, and 250–400 keV, respectively. (Third-to-bottom) Pi2 pulsations in the dusk sector. The time-MLT dependence of the local Pi2 onset is indicated by the dashed line.

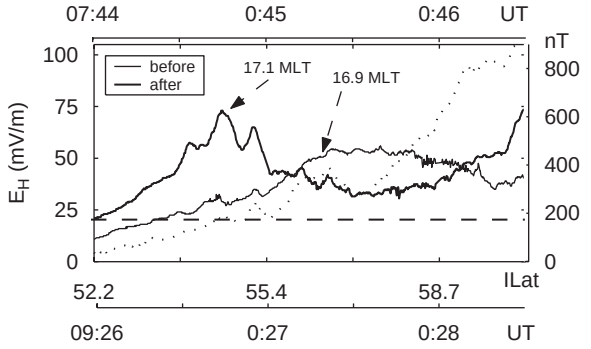

Fig. 4. The SAPS pattern near 17 MLT along two successive orbits of DMSP F13 before (UT is shown on the top) and after the substorm onset. The horizontal dashed line indicates the Farley–Buneman instability threshold. The dotted line shows deviation from the IGRF model of the post-onset eastward magnetic component ΔB_Z (the right axis).

shifted equatorward, the electric field intensified and became structured. Similar changes experienced also the SAPS observed by F11 (1830 MLT), F12 (20 MLT), and F14 (1930 MLT) ~15 min earlier and later than the above snapshots, respectively. Note that the available particle data from the DMSP satellites indicate that the post-onset equatorward boundary of the auroral zone was near 58° ILAT.

The horizontal dashed line in Fig. 4 indicates the threshold (E_{th}~20 mV/m) of the Farley–Buneman (FB) instability that generates field-aligned irregularities (FAI) in the E-region ionosphere (e.g., Farley, 1963). Indeed, sidelobe coherent backscatter from ~1-m FAI in the late-afternoon sector was observed by the incoherent scatter radar (ISR), which has the carrier frequency $f_0 = 150$ MHz and is located near Irkutsk (~47.1 MLat and MLT $\approx$ UT + 7). The temporal/spatial resolution of the backscatter observations was ~2-min/20-km, respectively. From general considerations it is clear that larger magnitudes of the electric field $E_0 > E_{th}$ should yield stronger backscatter. Foster and Erickson (2000) obtained the relation $E_0 \approx 2P_{\mathrm{cb}}(\mathrm{mV/m})/\mathrm{dB}$ for the Millstone Hill radar ($f_0 = 440$ MHz). Here $P_{\mathrm{cb}}(\Lambda(r), t) = 10\log_{10}[A(\Lambda(r), t)]\,\mathrm{dB}$ is the coherent backscatter power, corrected for variation of aspect

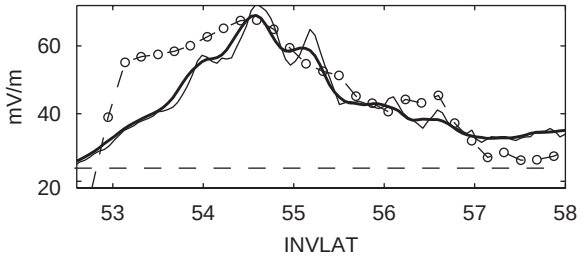

Fig. 5. The SAPS electric field (thin line) and its 3-s average (heavy line) vs. the (scaled) backscatter amplitude averaged over 09 : 25–09 : 30 UT (circles).

angle (at altitude 110 km) with range r, and $A(\Lambda, t)$ is the backscatter amplitude (cf. Foster et al., 1992). Such a mapping for the Irkutsk radar has not yet been established.

Fig. 5 shows the SAPS electric field after the onset and the (scaled) backscatter amplitude averaged over 09 : 25–09 : 30 UT (circles). Since the radar spatial resolution was ~20 km, the SAPS field was also averaged over 3 s or ~22.5 km (heavy line). Apparently, the radar and satellite observations are in good agreement near the SAPS maximum. Besides, as analyses show, the Foster and Erickson (2000) relation holds near the maximum. Thus, the Irkutsk ISR data can be safely used to specify the SAPS's dynamics. Variations of the corrected backscatter power $P_{cb}(\Lambda(r), t)$ are shown in Fig. 6 (the bottom panel). One can see that near 08 : 30 UT the backscatter power abruptly increased and its region shifted equatorward, indicating emerging over-threshold electric fields (cf. Erickson et al., 2002). This is consisitent with the enhanced eastward currents (poleward electric fields) at $\Lambda < 60^\circ$ in Fig. 2, although the large-scale MIT2 cannot distinguish the small-scale SAPS region.

In order to reduce possible correction-related errors, we also use relative amplitudes $\delta A_j(t) = \delta A(\Lambda_j, t) = A(\Lambda_j, t)/\max(A(\Lambda_j, T))$, where T is the period from 07 : 00 to 09 : 00 UT. The top panel in Fig. 6 shows variations of $\langle \delta A \rangle|_\Lambda$, i.e. $\delta A_j(t)$ averaged about Λ_j over the range of ~0.5°. One can see that near 08 : 24 UT weak scattering from $\Lambda > 55^\circ$ intensified, and in ~2−3 min the backscatter region began expanding equatorward. Overall, the observations suggest that the SAPS's perturbation in the afternoon sector followed the WTS arrival at the adjacent auroral region and developed within ~10 min after the substorm onset.

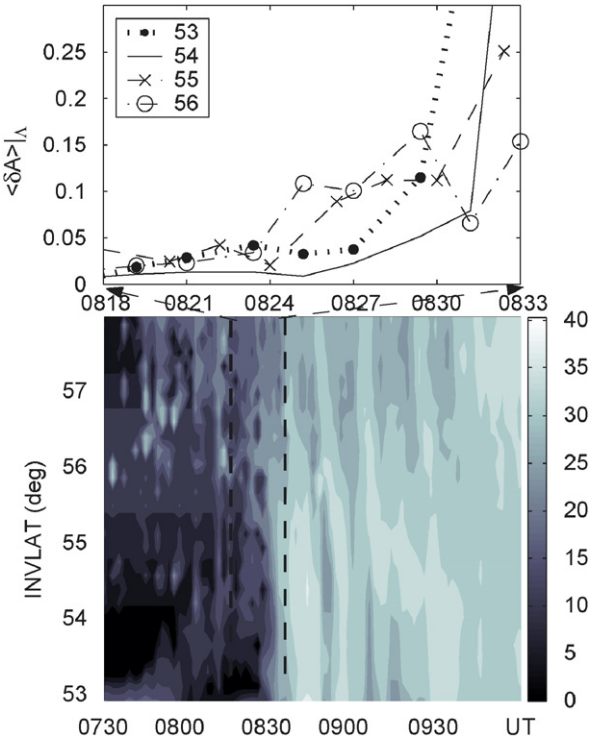

Fig. 6. Top: variations in the relative amplitude of backscatter from the ranges near $\Lambda = 53^\circ$, 54°, 55°, and 56°, respectively. Bottom: spatial–temporal variations of the corrected coherent backscatter power in the invariant latitude–time coordinates. Vertical dashed lines indicate a 15-min period after the onset.

3. Discussion

It is commonly accepted that the immediate cause of SAPS is the downward FAC derived from the product $\Gamma_\parallel = [\nabla \Pi \times \nabla P_{RC}] \cdot \mathbf{B}/B$. Here P_{RC} is the ring current pressure, Π is the flux tube volume, and $\mathbf{B}$ is the geomagnetic field (e.g., Vasyliunas, 1970). From numerical simulations it follows that the enhanced convection (dawn–dusk) electric field builds the ring current pressure on a slow, i.e. a few hours, timescale (e.g., Liemohn et al., 2001; Garner et al., 2004). However, Ganushkina et al. (2001) reported on the nose event, i.e. energetic ion enhancements at $L = 4-6$ exhibiting a 'nose' shape in the energy-time spectrograms (Smith and Hoffman, 1974), which was observed within one hour after the onset of a substorm.

In order to match the observations, Ganushkina et al. (2001) accounted for transient electromagnetic fields associated with the dipolarization process (e.g., Birn et al., 1997; Liou et al., 2001). This made it possible to move particles into the inner

magnetosphere within some tens of minutes (see also Ganushkina et al., 2005). Goldstein et al. (2005) explored the 'dipolarization pulse' or 'substorm injection' scenario to explain the post-onset ring current pressure buildup in the evening sector and westward moving ripples at the plasmapause, closely correlated with the FUV aurora. Apparently, the characteristic features of the post-onset SAPS development are consistent with these results. Furthermore, the magnetic observations suggest that the increase of $\Gamma_{\parallel}(P_{RC})$ at the duskside closely followed the WTS arrival at the adjacent plasma sheet. The time lag ~5 min behind the dispersionless ion injection at geosynchronous orbit implies the radial (inward) speed of ~70 km/s, i.e. within the range of typical inward velocities of the dipolarization pulse (e.g., Birn et al., 1997).

We argue that the pulse motion across **B** is essential for the formation of the SAPSWS. Actually, Mishin and Burke (2005) discussed the generation of the SAPSWS in terms of the current convective instability (Kadomtsev, 1965; Ossakow and Chaturvedi, 1979) developing at subauroral latitudes. The instability relies on FACs ($j_{\parallel}$) destabilizing the plasma configuration similar to that equatorward of the plasma sheet. Indeed, the RC pressure gradient at the inner edge is parallel to the centrifugal force acting on a particle in curved magnetic field lines. This is opposite to the condition of the Rayleigh–Taylor instability. If, however, the Doppler-shifted frequency $f - k_{\parallel} \cdot u_{\parallel}/(2\pi)$ is negative, the total wave energy turns to be negative too. Here $u_{\parallel}$ is the current velocity and $k_{\parallel}$ is the longitudinal component of the wave vector. As a result, the collisionless damping increases the wave energy, i.e. initial perturbations grow with time. Note that whenever magnetic observations were available during the SAPSWS events, downward FACs $>0.1\,\mu A/m^2$ were present (Mishin et al., 2003a, b).

Volkov and Maltsev (1986) derived the instability growth rate $\gamma \sim j_{\parallel}/(\Sigma_P B_I)$ in the Region 2 FACs near the plasma sheet boundary. Here Σ_P and B_I are the Pedersen conductivity and magnetic field strength in the conjugate ionosphere (subscript I), respectively. In the quasi-static approximation $j_{\parallel} = \nabla_{\perp}(\Sigma_P \mathbf{E}_I)$, the expression for γ can be reduced to $\sim \nabla_{\perp}\langle \mathbf{V}_W \rangle$, where $\langle \mathbf{V}_W \rangle$ is the average (dc) SAPS velocity. In addition, in the (dipolarization pulse) frame of reference, moving across **B** with the velocity $\mathbf{U}_{\perp}$, the wave frequencies are shifted by $\mathbf{k}_{\perp} \cdot \mathbf{U}_{\perp}/(2\pi)$, thus favoring the generation of short-scale perturbations (cf. Mishin, 1993). Further, the SAPS-associated FACs decrease with time, i.e. $j_{\parallel}(t) \to 0$ (e.g., Rich et al., 1980; Anderson et al., 1993). The presence of the factors $j_{\parallel}(t)$ and $\mathbf{U}_{\perp}$ suggests the occurrence of the SAPSWS during the post-onset period of (stormtime) substorms, in agreement with the observations.

It is worth noting that the ionospheric feedback is likely to amplify the instability growth (e.g., Streltsov and Mishin, 2003). Additional investigations are needed to address this problem, which is beyond the scope of this study.

4. Conclusion

Satellite, incoherent scatter radar, and ground magnetometer observations during the magnetic storm of 25 September 1998 specified the SAPS's response to a stormtime substorm. Following the substorm onset, the pre-existing SAPS in the afternoon sector moved equatorward and intensified within ~10 min. It is shown that this transition followed the arrival of the westward traveling surge at the adjacent auroral region. The observations indicate that the stormtime ring current responds to the substorm expansion on a rapid timescale, characteristic for the dipolarization pulse and WTS development. We propose a scenario for the generation of the post-onset SAPS-wave structures by the current convective instability developing at the front of the RC ion cloud picked up by the dipolarization pulse.

Acknowledgments

EVM thanks W.J. Burke for discussions. The Irkutsk ISR is operated by the Institute of Solar-Terrestrial Physics, SB RAS. The ISR data were provided by A.P. Potekhin and J.C. Foster. The LANL satellites particle data were provided by G.D. Reeves. CANOPUS magnetic data were obtained through the Canadian Space Agency CANOPUS Web site. The 210 MM magnetometer chain data were provided by K. Shiokawa. This research was supported in part by AFRL contract F19628-02-C-0012 with Boston College.

References

Akasofu, S.-I., 1977. Physics of Magnetospheric Substorms. Reidel, Dordrecht.

Anderson, P., Hanson, W., Hellis, R., Graven, J., Baker, D., Frank, L., 1993. A proposed production model of rapid subauroral ion drifts and their relationship to substorm evolution. Journal of Geophysical Research 98, 6069–6079.

Basu, Su., Basu, Sa., Valladares, C., Yeh H.-C., Su, S.-Y., MacKenzie, E., Sultan, P.J., Aarons, J., Rich, F.J., Doherty, P., Groves, K.M., Bullett, T.W., 2001. Ionospheric effects of major magnetic storms during the International Space Weather Period of September and October 1999: GPS observations, VHF/UHF scintillations and in situ density structures at middle and equatorial latitudes. Journal of Geophysical Research 106, 30,389–30,413, doi:10.1029/2001JA001116.

Birn, J., Thomsen, M., Borovsky, J., Reeves, G., McComas, D., Belian, R., Hesse, M., 1997. Substorm ion injections: geosynchronous observations and test particle orbits in three-dimensional dynamic MHD fields. Journal of Geophysical Research 102, 2309.

Erickson, P., Foster, J., Holt, J., 2002. Inferred electric field variability in the polarization jet from Millstone Hill *E* region coherent scatter observations. Radio Science 37 (2), 1027.

Farley, D., 1963. A plasma instability resulting in field aligned irregularities in the ionosphere. Journal of Geophysical Research 68, 6083–6097.

Foster, J., Burke, W., 2002. A new categorization for subauroral electric fields. EOS Transactions AGU 83, 393.

Foster, J., Erickson, P., 2000. Simultaneous observations of *E*-region coherent backscatter and electric field amplitude at *F*-region heights with the Millstone Hill UHF radar. Geophysical Research Letters 27, 3177–3180.

Foster, J., Erickson, P., Lind, F., Rideout, W., 2004. Millstone Hill coherent-scatter radar observations of electric field variability in the subauroral polarization stream. Geophysical Research Letters 31, L21803.

Foster, J., Tetenbaum, D., delPozo, C., St-Maurice, J.-P., Moorcroft, D., 1992. Aspect angle variations in intensity, phase velocity, and altitude for high-latitude 34-cm *E* region irregularities. Journal of Geophysical Research 97, 8601.

Galperin, Y., Ponomarev, Y., Zosimova, A., 1974. Plasma convection in the polar ionosphere. Annales Geophysicae 30, 1–7.

Ganushkina, N., Pulkkinen, T., Bashkirov, V., Baker, D., Li, X., 2001. Formation of intense nose structures. Geophysical Research Letters 28, 491–494.

Ganushkina, N., Pulkkinen, T., Fritz, T., 2005. Role of substorm-associated impulsive electric fields in the ring current development during storms. Annales Geophysicae 23, 579–591.

Garner, T., Wolf, R., Spiro, R., Burke, W., Fejer, B., Sazykin, S., Roeder, J., Hairston, M., 2004. Magnetospheric electric fields and plasma sheet injection to low L-shells during the 4–5 June 1991 magnetic storm: comparison between the rice convection model and observations. Journal of Geophysical Research 109, A202214.

Goldstein, J., Burch, J., Sandel, B., Mende, S., C:son Brandt, P., Hairston, M., 2005. Coupled response of the inner magnetosphere and ionosphere on 17 April 2002. Journal of Geophysical Research 110, A03205.

Kadomtsev, B., 1965. Plasma Turbulence. Academic Press, NY, pp. 11–15.

Ledvina, B., Makela, J., Kintner, P., 2002. First observations of intense GPS L1 amplitude scintillations at midlatitude. Geophysical Research Letters 29 (14), doi:10.1029/2002GL014770.

Liemohn, M., Kozyra, J., Thomsen, M., Roeder, J., Lu, G., Borovsky, J., Cayton, T., 2001. Dominant role of the asymmetric ring current in producing the stormtime Dst*. Journal of Geophysical Research 106, 10883.

Liou, K., Meng, C.-I., Newell, P., Takahashi, K., Ohtani, S.-I., Lui, A., Brittnacher, M., Parks, G., 2000. Evaluation of low-latitude Pi2 pulsations as indicators of substorm onset using Polar ultraviolet imagery. Journal of Geophysical Research 105, 2495–2505.

Liou, K., Meng, C.-I., Newell, P., Lui, A., Reeves, G., Belian, R., 2001. Particle injections with auroral expansions. Journal of Geophysical Research 106, 5873–5881.

Maynard, N., Aggson, T., Heppner, J., 1980. Magnetospheric observation of large subauroral electric fields. Geophysical Research Letters 7, 881.

Mishin, V.M., 1991. The magnetogram inversion technique: applications to the problem of magnetospheric substorms. Space Science Review 57, 237–337.

Mishin, V.V., 1993. Acceleration motions of the magnetopause as a trigger of the Kelvin-Helmholtz instability. Journal of Geophysical Research 98, 21365–21371.

Mishin, V.M., Russell, C., Saifudinova, T., Bazarzhapov, A., 2000. Study of weak substorms observed during December 8 1990, Geospace Environment Modeling campaign: timing of different types of substorm onsets. Journal of Geophysical Research 105, 23263–23276.

Mishin, E., Burke, W., 2005. Stormtime coupling of the ring current, plasmasphere and topside ionosphere: electromagnetic and plasma disturbances. Journal of Geophysical Research 110, A07209.

Mishin, E., Foster, J., Potekhin, A., Rich, F., Schlegel, K., Yumoto, K., Taran, V., Ruohoniemi, J., Friedel, R., 2002. Global ULF disturbances during a stormtime substorm on 25 September 1998. Journal of Geophysical Research 107 (A12), 1486.

Mishin, E., Burke, W., Huang, C., Rich, F., 2003a. Electromagnetic wave structures within subauroral polarization streams. Journal of Geophysical Research 108 (A8), 1309.

Mishin, E., Burke, W., Basu, S., Basu, Sh., Kintner, P., Ledvina, B., 2003b. Stormtime ionospheric irregularities in SAPS-related troughs: cause of GPS scintillations at mid latitudes, in: EOS Transactions AGU 84(46), Fall Meeting Supplementary Abstract SH52A-07, San Francisco, USA.

Mishin, E., Burke, W., Viggiano, A., 2004. Stormtime subauroral density troughs: ion-molecule kinetics effects. Journal of Geophysical Research 109, A10301.

Ossakow, S., Chaturvedi, P., 1979. Current convective instability in the diffuse aurora. Geophysical Research Letters 6, 332–335.

Pytte, T., McPherron, R., Kokubun, S., 1976. The ground signatures of the expansion phase during multiple onset substorms. Planetary and Space Science 24, 1115–1132.

Rich, F., Burke, W., Kelley, M., Smiddy, M., 1980. Observations of field-aligned currents in association with strong convection electric fields at subauroral latitudes. Journal of Geophysical Research 85, 2335.

Rothwell, P., Silevitch, M., Block, L., 1984. A model for the propagation of the westward traveling surge. Journal of Geophysical Research 89, 8941–8948.

Smith, P.H., Hoffman, R.A., 1974. Direct observations in the dusk hours of the characteristics of storm time ring current particles during the beginning of magnetic storms. Journal of Geophysical Research 79, 964–967.

Spiro, R., Heelis, R., Hanson, W., 1979. Rapid subauroral ion drifts observed by Atmospheric Explorer C. Geophysical Research Letters 6, 657–660.

Streltsov, A., Mishin, E., 2003. Numerical modeling of localized electromagnetic waves in the nightside subauroral zone. Journal of Geophysical Research 108 (A8), 1332.

Thomsen, M., Birn, J., Borovsky, J., Morzinski, K., McComas, D., Reeves, G., 2001. Two-satellite observations of substorm injections at geosynchronous orbit. Journal of Geophysical Research 106, 8405–8416.

Tsyganenko, N., Singer, H., Kasper, J., 2003. Storm-time distortion of the inner magnetosphere: how severe can it get? Journal of Geophysical Research 108 (A5), 1209.

Yumoto, K., 210MM Magnetic Observations Group, 1996. The STEP 210 magnetic meridian network project. Journal of Geomagnetism and Geoelectricity 48, 1297–1309.

Vasyliunas, V., 1970. Mathematical models of magnetospheric convection and its coupling to the ionosphere. In: McCormac, B.M. (Ed.), Particles and Fields in the Magnetosphere. Reidel, Dordrecht, Holland, p. 60.

Volkov, M., Maltsev, Yu., 1986. A slot instability of the inner boundary of the plasma layer. Geomagnetism and Aeronomy 26, 671–673.